Monolayer MoSe 2 Grown by Chemical Vapor Deposition for Fast Photodetection

Monolayer $MoSe_2$ Grown by Chemical Vapor deposition for Fast Photodetection

Yung-Huang Chang[1^], Wenjing Zhang[2,3^], Yihan Zhu[4], Yu Han[4], Jiang Pu[5], Jan-Kai Chang[6], Wei-Ting Hsu[7], Jing-Kai Huang[1], Chang-Lung Hsu[1], Ming-Hui Chiu[4], Taishi Takenobu[5,8], Henan Li[9], Chih-I Wu[6], Wen-Hao Chang[7], Andrew Thye Shen Wee[2] and Lain-Jong Li[1,4]*

[1]*Institute of Atomic and Molecular Sciences, Academia Sinica, Taipei, 11529, Taiwan*.

[2]*Department of Physics, National University of Singapore, Singapore 117542, Singapore.*

[3]*SZU-NUS Collaborative Innovation Center for Optoelectronic Science & Technology, Key Laboratory of Optoelectronic Devices and Systems of Ministry of Education, Guangdong Province, Shenzhen University, Shenzhen 518060, China.*

[4]*Physical Science and Engineering Division, King Abdullah University of Science and Technology, Thuwal 23955-6900, Saudi Arabia.*

[5]*Department of Advanced Science and Engineering, Waseda University, Tokyo 169-8555, Japan*

[6]*Institute of Photonics and Optoelectronics and Department of Electrical Engineering, National Taiwan University, Taipei 10617, Taiwan.*

[7]*Department of Electrophysics, National Chiao Tung University, Hsinchu 30010, Taiwan.*

[8]*Department of Applied Physics, Kagami Memorial Laboratory for Material Science and Technology, Waseda University, Tokyo 169-8555, Japan.*

[9]*School of materials science and engineering, Nanyang Technological University, Singapore 639798, Singapore.*

RECEIVED DATE ()

^These authors contributed equally

*Address correspondence to L.J.Li: lance.sinica@gmail.com

ABSTRACT

Monolayer molybdenum disulfide (MoS_2) has become a promising building-block in optoelectronics for its high photosensitivity. However, sulfur vacancies and other defects significantly affect the electrical and optoelectronic properties of monolayer MoS_2 devices. Here, highly crystalline molybdenum diselenide ($MoSe_2$) monolayers have been successfully synthesized by the chemical vapor deposition (CVD) method. Low temperature photoluminescence comparison for MoS_2 and $MoSe_2$ monolayers reveals that the $MoSe_2$ monolayer shows a much weaker bound exciton peak; hence, the phototransistor based on $MoSe_2$ presents a much faster response time (< 25ms) than the corresponding 30 sec for CVD MoS_2 monolayer at room temperature in ambient. The images obtained from transmission electron microscopy indicate that the MoSe exhibits lower amounts of defects than MoS_2. This work provides the fundamental understanding for the differences in optoelectronic behaviors between $MoSe_2$ and MoS_2, and is useful for guiding future designs in 2D material-based optoelectronic devices.

KEYWORDS: Transition metal dichalcogenides; Photoresponse; $MoSe_2$; MoS_2; Two-dimensional materials

Transition metal dichalcogenides (TMD) with the formula MX_2, where M is a transition metal (Mo, W and so on) and X is a chalcogen (S, Se or Te), have attracted much attention due to their layer structure and semiconducting properties.[1-6] These two-dimensional (2d) materials are in the form of X–M–X, where a plane of metal atoms is sandwiched between two planes of chalcogen atoms by covalent interaction, and different layers are held together by van der Waals interactions.[7,8] These layer materials exhibit many distinctive characteristics such as outstanding flexibility,[9] moderate carrier mobility,[10,11] and layer-dependent electronic and optical properties.[12-20] Thus, the TMD materials can serve as transparent and flexible field-effect transistors (FETs),[21-24] photodetectors,[25] photovoltaic cells,[26,27] light-emitting diodes[28,29] and catalysts.[30-32] In particular, TMD materials have been reported to absorb up to 5−10% of incident sunlight within a thickness less than 1 nm, which is about 1 order of magnitude higher absorption than GaAs and Si.[26] The phototransistors based on monolayer MoS_2 show outstanding photoresponsivity even up to a few thousand A/W.[25,33] Recently, a graphene/MoS_2 hybrid phototransistor was demonstrated to be able to provide a photogain of more than 10^8.[34] However, the long response time of 4 to 30s for monolayer MoS_2-based phototransistors, caused by persistent photocarriers generated from trapped defects or charged impurity states,[25,33,34] limits their application for fast photon detection.

Recently, monolayer $MoSe_2$ has started to gain attention since it has many interesting electronic and optical properties similar to monolayer MoS_2, such as a direct band gap, strong photoluminescence, and a large exciton binding energy.[35-41] It is known that sulfur defects in MoS_2 monolayer greatly affect the electronic transport and optical properties. Therefore, it would be meaningful to carefully compare the properties of monolayer

MoS_2 and $MoSe_2$. One important question is whether $MoSe_2$ monolayer grown by chemical vapor deposition (CVD) exhibits better optoelectronic characteristics. In this study, we synthesized monolayer $MoSe_2$ on sapphire by the gas phase reaction between MoO_3 and Se powders in a hot-wall tube furnace system, using a CVD method which has been reported elsewhere.[4,6] X-ray Photoemission Spectroscopy (XPS) and Transmission Electron Microscopy (TEM) measurements confirm that the $MoSe_2$ film is highly crystalline. By comparing the electrical devices fabricated with these two monolyers, we demonstrate that both MoS_2 and $MoSe_2$ monolayers exhibit a comparable mobility value for the electron transport. It is also noteworthy that electrical and ultraviolet photoemission spectroscopy (UPS) measurements demonstrate that MoS_2 is heavily *n*-doped but $MoSe_2$ is less *n*-doped. Low temperature photoluminescence study reveals that $MoSe_2$ monolayer has a much weaker bound exciton peak, indirectly suggesting that the $MoSe_2$ monolayer possesses fewer defects or impurities. Most interestingly, the CVD $MoSe_2$ monolayer exhibits a much faster response time (< 25ms) than MoS_2, making it superior for fast photodetection applications.

Results and Discussion

Synthesis of $MoSe_2$ Monolayer:

The experimental set-up for growing monolayer $MoSe_2$ using MoO_3 and Se powder precursors in a hot-wall CVD system is schematically illustrated in Figure 1(a). Hydrogen was introduced as a reducing agent during the growth process.[5] The morphology of the $MoSe_2$ grown on sapphire substrates varies with the distance of the

substrate from the MoO_3 source, as shown in Figures 1(b)-(c). The optical micrograph (OM) in Figure 1(b) shows that the sparsely distributed triangular crystals (lateral size ~ 5 micron) are found in most areas of the substrate located furthest from the MoO_3 source. When the substrate is close to the MoO_3 source, the nucleation density becomes much higher such that these small domains easily merge to form a continuous film, as shown in the atomic force microscopy (AFM) image in Figure 1(c). Moreover, the cross sectional height profile in Figure 1(d) shows that the thickness of the $MoSe_2$ film is ~0.7 nm, corresponding to a monolayer and consistent with published monolayer thickness.[6,37] Figure 1(e) shows the OM of the $MoSe_2$ monolayer. In addition to the $MoSe_2$ monolayer, we occasionally observe the growth of 2nd layer $MoSe_2$ on top of some monolayer flakes, as shown in Figure S1. The occasionally found $MoSe_2$ 2nd layers are normally in the areas with high substrate roughness or with some particles, likely due to that the rough surfaces or particles are able to assist the nucleation of the 2nd layer.

Structural Characterization of $MoSe_2$:

The layer dependence of Raman features has been reported for TMDs such as MoS_2, $MoSe_2$ and WSe_2.[7,16,38,40] In Figure 2(a) the synthesized monolayer $MoSe_2$ exhibits two characteristic peaks located at 241.2 cm^{-1} and 286.7 cm^{-1}, associated with the out-of-plane A_{1g} mode and in-plane E^1_{2g} mode respectively.[6,35] Furthermore, the Raman peak at ~353 cm^{-1}, which has been demonstrated to relate to the interlayer interaction, is not observed in our monolayer $MoSe_2$.[38] This suggests that the CVD synthesized $MoSe_2$ is indeed one monolayer. Figure 2(b) displays the PL spectrum for monolayer $MoSe_2$. Only a strong peak located at 793 nm is observed, attributed to the direct band gap emission from A excitons.[6,35,37] It is noted that the indirect gap emission is absent in the monolayer

and the strong A exciton emission from the monolayer is in good agreement with a recent report.[38,41] In addition, the XPS spectra for the CVD synthesized monolayer $MoSe_2$ in Figures 2(c) and 2(d) confirm the stoichiometry of $MoSe_2$. The peaks at 228.8 eV and 232 eV are attributed to the doublet Mo $3d_{5/2}$ and Mo $3d_{3/2}$ binding energies respectively for Mo^{4+}.[42,43] The peaks corresponding to the Se $3d_{5/2}$ and Se $3d_{3/2}$ orbitals of divalent selenide ions (Se^{2-}) are observed at 54.4 eV and 55.2 eV.[42,43] Aberration-corrected high-resolution TEM (HRTEM) images demonstrate a high crystallinity of monolayer $MoSe_2$, in which the Se and Mo atomic columns can be directly identified (Figures 2(e) and 2(f)). The remarkable contrast difference between Se and Mo is in good agreement with the simulated HRTEM image for monolayer $MoSe_2$ (Figure 2(f)). The lattice constant of the 2-D hexagonal lattice is measured both directly from the image and the corresponding Fourier transform and determined to be a = 0.323 nm, consistent with that of bulk $MoSe_2$.

Electric Double Layer Transistors:

The electrical characteristics of the electric double layer transistors (EDLTs) were measured directly for the monolayer $MoSe_2$ films on sapphire substrates. The detailed description of EDLT fabrication was reported in previous studies[3,5] and illustrated in Figure S2. The output characteristics for the $MoSe_2$ devices are also shown in Figure S2. Figure 3(a) shows the OM top view image of the $MoSe_2$ EDLT, where the channel width and length are 90 μm and 1000 μm, respectively. Figure 3(c) displays the *p*- and *n*-channel drain current as a function of the reference voltage V_R for monolayer $MoSe_2$ EDLT at the applied drain voltage V_D = - 0.1 V and 0.1 V, respectively. Note that V_R is the measured voltage between the electrolytes and $MoSe_2$, i.e. the voltage for the electric double layer on $MoSe_2$ surfaces. Since the gate voltage applied on the top Pt metal is

partially consumed by the electric double layer on the gate electrode, V_R is used instead for the gate dependence measurements. Although some reports have claimed that $MoSe_2$ is an *n*-type semiconductor,[44] we clearly observe an ambipolar transport behavior instead since the electric double layer exhibits a higher gating efficiency. Figure 3(c) shows that the threshold voltage for the *n*-channel is 0.64 V in the forward scan, smaller than the 1.46 V value for the *p*-channel, indicating that the $MoSe_2$ is an *n*-type preferred ambipolar semiconductor. However, a unipolar *n*-type electrical characteristic is presented for MoS_2 using the same EDLT technology as shown in Figure 3(b). Furthermore, we didn't observe any hole transport current in the same negative gate voltage range (-1.6V-0V) for MoS_2. The field-effect mobility was calculated using the standard formula in the linear region, $\mu = (L/WC_iV_D)\cdot(\Delta I_D/\Delta V_R)$, where μ is the field-effect mobility, W is the channel width, V_D is the drain voltage, C_i is the measured specific capacitance of the ion gel, L is the channel length and I_D is the drain current. The highest carrier mobility obtained for the $MoSe_2$ monolayer is 23 cm^2/Vs for electron transport and 15 cm^2/Vs for hole transport. For the MoS_2 monolayer, the electron mobility is around 17 cm^2/Vs. As shown in the insets of Figures 3(b)-3(d) , the current on-off ratio is as high as 10^4 ~10^5 for both $MoSe_2$ and MoS_2. The comparative EDLT measurement results for both $MoSe_2$ and MoS_2 are listed in Table 1. In brief, $MoSe_2$ exhibits a similar electron mobility value and on-off current ratio compared with MoS_2, which also makes it a promising candidate for FET applications.

Ultraviolet Photoemission Spectroscopy (UPS):

UPS is used to explore the energy level alignment with respect to the Fermi energy (E_F). The MoS_2 and $MoSe_2$ monolayers are separately transferred onto Si substrates coated

with 60 nm thermally evaporated Au. The Au layer serves as a reference for E_F, assigned to 0 eV.[45,46] As shown in Figure 4(a), the valence band (E_V) for MoS_2 and $MoSe_2$ on Au/Si substrates is respectively located at 1.75 eV and 1.20 eV below E_F by linearly extrapolating the leading edge of the spectrum to the baseline. In addition, the work function (Φ) can be calculated using $\Phi = h\nu - E_{onset}$, where $h\nu$ is the incident photon energy (40.8 eV) and E_{onset} is the onset level related to the secondary electrons, as shown in Figure 4(b).[47] Hence, the Φ for MoS_2 and $MoSe_2$ on Au/Si substrates is 4.20 eV and 4.27 eV, respectively. Note that the work function value obtained for monolayer MoS_2 is consistent with several other reports.[48-51] In addition, the optical band gaps of the CVD monolayer MoS_2 and $MoSe_2$ are determined to be ~1.83 eV and ~1.51 eV respectively from the absorption spectra (Figure S3). Thus, the energy band diagrams of CVD monolayer MoS_2 and $MoSe_2$ relative to the Fermi level E_F of gold films can be illustrated in Figures 4(c) and 4(d). The energy separation ΔE between the conduction band of MoS_2 and the E_F of Au is ~0.08eV, indicating that CVD monolayer MoS_2 is heavily *n*-doped, consistent with unipolar *n*-type electrical transport behavior. On the other hand, the energy separation ΔE between the conduction band of $MoSe_2$ and the E_F of Au is ~0.31eV, indicating that the CVD monolayer $MoSe_2$ is slightly *n*-doped, consistent with the *n*-type preferred ambipolar electrical transport behavior.

Optical Properties:

To examine the gate dependent photoresponse characteristics, the MoS_2 and the $MoSe_2$ films are respectively transferred onto 300 nm SiO_2/Si substrates, and the phototransistors patterned using standard photolithography. Figure S4 shows the optical image of the interdigitated electrodes used, where the contact metal layers, 10 nm Ti and 80 nm Au,

are deposited by thermal evaporation. 532 nm and 650 nm CW lasers are used as the light sources to study the MoS_2 and $MoSe_2$ phototransistors. Figure 5(a) presents the typical transport curves of the two phototransistors in the dark and under illumination. In the dark, the *n*-channel subthreshold voltage V_{th} of the $MoSe_2$ and MoS_2 is ~ 7V and ~ -46V respectively, corroborating that the MoS_2 on SiO_2 is much more heavily *n*-doped. The mobilities of $MoSe_2$ and MoS_2 transistors are ~0.012 cm^2/Vs at V_g=60V (V_g-V_{th}=53V) and ~0.021 cm^2/Vs at V_g=17V (V_g-V_{th}=53V), respectively. Compared with the devices on sapphire, the mobilities of the devices on SiO_2 is about 3 orders of magnitude lower, which may be caused by several factors including the possible degradation by transfer processes, the scattering effect from charge impurities added during the transfer process, and damage caused by patterning. Under illumination at power density of ~ 0.31 and 0.59 W/cm^2, the OFF state currents of both devices increase by ~3 orders of magnitude. The photo gain (G), given by $G=hvI_{ph}/(\eta eP_0)$,[33] is an index to quantify the conversion efficiency of incident photons to photogenerated carriers, where I_{ph} is the net photocurrent, P_0 is the absorbed laser power, h is Planck's constant, e is the charge of an electron, and v is the frequency of incident light. Assuming η=100%, the photo gain of the MoS_2 phototransistors is ~0.2, much higher than $\sim 5 \times 10^{-4}$ of the $MoSe_2$ phototransistor in the OFF state. The $MoSe_2$ band diagrams in Figures 4(c) and 4(d) indicate that the electron Schottky barrier of $MoSe_2$ is higher,[52] resulting in the smaller photo gain of $MoSe_2$ on SiO_2. This also accounts for the lower OFF state dark current for $MoSe_2$ (~10^{-12} A vs. the ~10^{-10} A for MoS_2).

Figures 5(c) and 5(d) show the time-resolved photocurrent for monolayer $MoSe_2$ and MoS_2 films, respectively, under ON/OFF light illumination at V_{ds} = 1 V in ambient. A

fast rise and decay response time shorter than ~25 ms for $MoSe_2$ is observed. However, the photocurrent of the MoS_2 phototransistors takes more than 30s to saturate and decay. The persistent photocurrent is normally attributed to defect or charge impurity states inside the band gap.[53] Figures 5(e) and 5(f) show the photoluminescence (PL) spectra of the monolayer $MoSe_2$ and MoS_2 at room and low temperatures. We observe only one peak at room temperature, ~1.55 eV for the $MoSe_2$ and ~1.88 eV for the MoS_2, corresponding to the direct band-to-band A excitonic transition. The peak intensity for monolayer $MoSe_2$ at room temperature is stronger than that of monolayer MoS_2, and the full width at half maximum (FWHM) of ~42 meV for monolayer $MoSe_2$ is smaller than the ~51 meV value of monolayer MoS_2. When the temperature decreases to 12K, an additional sub-bandgap emission at the low energy side between 1.4 to 1.9 eV appears for the monolayer CVD MoS_2, which could be attributed to the defect or charge impurity states.[15,53] Due to the additional binding to defects or charge impurities, the energy of the bound exciton peak is lower than that of the free exciton peak.[15] The large width of the bound exciton peak indicates the presence of different kinds of defects or charge impurity sites since different binding energies are needed. In contrast, no sub-bandgap emission is observed at the low energy side for the CVD $MoSe_2$ monolayer, implying better crystalline quality and fewer defects or charge impurity states, thus resulting in higher band-to-band free exciton recombination rates. Some reports have pointed out that the persistent photoconductance arise from the defects or charge impurity states inside the bandgap.[33,54,55] Hence, the extra photogenerated carriers in the MoS_2 arising from the defects or charge impurity states could be responsible for its slow light response time. Figure S5 shows the HRTEM image for the CVD MoS_2 monolayers with abundantly

disordered atom arrangement highlighted by dash circles, which is in clear contrast to the HRTEM for CVD $MoSe_2$ in Figures 2(e) and 2(f).

Moreover, the CVD MoS_2 shows significantly lower stability in ambient, where its PL intensity normally decays in 2 or 3 days. We notice that the shelf life time can be increased to more than one week if the sample is stored in a dry box, indicating that the moisture may react or catalyze the formation of defects in MoS_2. By contrast, PL measurements suggest that the CVD $MoSe_2$ monolayer exhibits a much longer shelf life time, typically more than 4 weeks, in the same ambient storage condition. These observations are also in line with a relatively larger amount of defects in MoS_2 revealed by TEM.

Conclusions

In conclusion, we have synthesized crystalline monolayer $MoSe_2$ by the gas phase selenization of MoO_3 in a hot-wall CVD chamber. From the analyses of EDLT and UPS measurements, the $MoSe_2$ exhibits a slight *n*-type preferred ambipolar behavior, while the MoS_2 shows heavily *n*-doped electrical characteristics. In addition, the defect-less crystalline structure for the $MoSe_2$ is identified through the low temperature PL, whereas relatively abundant defects occur in MoS_2. This study shows that CVD synthesized monolayer $MoSe_2$ has great potential in flexible transparent optoelectronic applications.

Methods

Growth of $MoSe_2$ monolayers: The MoO_3 powders (0.025-0.3 g) were placed in a ceramic boat located in the heating zone center of the furnace. The Se powders were

placed in a separate quartz boat at the upper stream side maintained at 270 ºC during the reaction. The sapphire substrates for growing $MoSe_2$ were placed at the downstream side near MO_3 powders, where the Se and MoO_3 vapors were brought to the targeting sapphire substrates by an Ar/H_2 flowing gas (Ar = 40-70 sccm, H_2 = 10 sccm, chamber pressure = 25-350 Torr). The center heating zone was heated to 700-900 ºC at a ramping rate 15 ºC/min. After reaching growth temperature, the heating zone was kept for 15 minutes and the furnace was then naturally cooled down to room temperature.

Fabrication of EDLT devices: For the source and drain electrodes, Au contacts with Ni adhesion layers (70 nm / 2 nm) were thermally deposited onto the surface of the $MoSe_2$ films. The ion gels, a mixture of a triblock copolymer, poly(styrene-block-methyl methacrylate-block-styrene) (PS-PMMA-PS; *MPS* = 4.3 kg/mol, *MPMMA* = 12.5 kg/mol, *Mw* = 21.1 kg/mol), and an ionic liquid, 1-ethyl-3-methylimidazoliumbis(trifluoromethylsulfonyl)imide ([EMIM][TFSI]) in an ethyl propionate solution, are used as the top gate dielectrics. Note that the weight ratio of the polymer, ionic liquid, and solvent was maintained at 0.7:9.3:20. This solution was drop-casted onto and cover the surfaces of $MoSe_2$ film and the source and drain electrodes. The transistor channel was then covered with a thin Pt foil (thickness of 0.03 mm) to form the top-gate electrode. Finally, a thin gold wire was inserted into the gel films, in between the channel and top gate metal, as the reference electrode. All electrical characterizations were performed using a semiconductor parameter analyzer (Agilent E5270) in a shield probe station inside an N_2-filled glove box.

Characterizations: Photoluminescence spectra were excited by green light laser with 532 nm wavelength and 0.9 N.A. of objective (spot size: 0.7 μm). Raman spectra were collected in a NT-MDT confocal Raman microscopic system (laser wavelength 473 nm and laser spot size ~0.5 μm). The Si peak at 520 cm^{-1} was used as reference for wavenumber calibration. The AFM images were performed in a Veeco Dimension-Icon system. Chemical configurations were determined by X-ray photoelectron spectroscope (XPS, Phi V5000). XPS measurements were performed with an Mg Kα X-ray source on the samples. The energy calibrations were made against the C 1s peak to eliminate the charging of the sample during analysis. The valence band UPS were performed using He

I (21.2 eV) and He II (40.8 eV) photon lines as excitation sources, and the photoelectrons were analyzed with a hemispherical analyzer with an overall resolution of 0.05 eV. The absorbance spectra were obtained using a JASCO-V-670 UV-vis spectrophotometer. The MoSe2 films were transferred onto a copper grid for TEM observation. HRTEM imaging was performed on an aberration-corrected and monochromated G^2 cubed Titan 60-300 electron microscope under 60 kV. The electrical measurements were performed using a Keithley semiconductor parameter analyzer, model 4200-SCS. All the measurements were achieved at room temperature in ambient air. The continuous wavelength 532 nm and 650 nm lasers were used to measure the photoresponse of the devices, and the spot size was ~1 mm.

ACKNOWLEDGMENT: This research was supported by Academia Sinica, National Science Council Taiwan (102-2119-M-001-005) and AFOSR-BRI USA. T.T. was partially supported by the Funding Program for the Next Generation of World-Leading Researchers and Grants-in-Aid from MEXT (26107533 "Science of Atomic Layers" and 25000003 "Specially Promoted Research")

Supporting Information Available:

Raman spectra are included. This material is available free of charge *via* the Internet at http://pubs.acs.org.

REFERENCES

1. Chhowalla, M.; Shin, H. S.; Eda, G.; Li, L.-J.; Loh, K. P.; Zhang, H. The Chemistry of Two-Dimensional Layered Transition Metal Dichalcogenide Nanosheets. *Nat. Chem.* **2013**, *5***,** 263–275.
2. Wang, Q. H.; Kalantar-Zadeh, K.; Kis, A.; Coleman, J. N.; Strano, M. S. Electronics and Optoelectronics of Two-Dimensional Transition Metal Dichalcogenides. *Nat. Nanotechnol.* **2012**, *7*, 699–712.
3. Lee, Y. H.; Zhang, X. Q.; Zhang, W.; Chang, M. T.; Lin, C. T.; Chang, K. D.; Yu, Y.-

C.; Wang, T. W.; Chang, C.-S.; Li, L. J. *et al.* Synthesis of Large-Area MoS_2 Atomic Layers with Chemical Vapor Deposition. *Adv. Mater.* **2012**, *24*, 2320−2325.
4. Lee, Y.-H.; Yu, L.; Wang, H.; Fang, W.; Ling, X.; Shi, Y.; Lin, C.-T.; Huang, J.-K.; Chang, M.-T.; Chang, C.-S. *et al.* Synthesis and Transfer of Single Layer Transition Metal Disulfides on Diverse Surfaces *Nano Lett.* **2013**, *13*, 1852−1857.
5. Huang, J.-K.; Pu, J.; Hsu, C.-L.; Chiu, M.-H.; Juang, Z.-Y.; Chang, Y.-H.; Chang, W.-H.; Iwasa, Y.; Takenobu, T.; Li, L.-J. Large-Area Synthesis of Highly Crystalline WSe_2 Monolayers and Device Applications. *ACS Nano*, **2014**, *8*, 923–930.
6. Shaw, J. C.; Zhou, H.; Chen, Y.; Weiss, N. O.; Liu, Y.; Huang, Y.; Duan, X. Chemical Vapor Deposition Growth of Monolayer $MoSe_2$ Nanosheets. *Nano Res.* **2014**, *7*, 1−7.
7. Huang, X.; Zeng, Z; Zhang, H. Metal Dichalcogenide Nanosheets: Preparation, Properties and Applications. *Chem. Soc. Rev.* **2013**, *42***,** 1934–1946.
8. Ataca, C.; Sahin, H.; Ciraci, S. Stable, Single-Layer MX_2 Transition-Metal Oxides and Dichalcogenides in a Honeycomb-Like Structure. *J. Phys. Chem. C* **2012**, *116***,** 8983−8999.
9. Pu. J.; Yomogida, Y.; Liu, K.-K.; Li, L.-J.; Iwasa, Y.; Takenobu, T. Highly Flexible MoS_2 Thin-Film Transistors with Ion Gel Dielectrics. *Nano Lett.* **2012**, *12***,** 4013–4017.
10. Radisavljevic, B.; Radenovic, A.; Brivio, J.; Giacometti, V.; Kis, A. Single-Layer MoS_2 Transistors. *Nat. Nanotechnol.* **2011**, *6***,** 147−150.
11. Radisavljevic, B.; Whitwick, M. B.; Kis, A. Integrated Circuits and Logic Operations Based on Single-Layer MoS_2. *ACS Nano* **2011**, *5***,** 9934−9938.
12. Splendiani, A.; Sun, L.; Zhang, Y.; Li, T.; Kim, J.; Chim, C.-Y.; Galli, G.; Wang, F. Emerging Photoluminescence in Monolayer MoS_2. *Nano Lett.* **2010**, *10***,** 1271−1275.
13. Mak, K. F.; Lee, C.; Hone, J.; Shan, J.; Heinz, T. F. Atomically Thin MoS_2: a New Direct-Gap Semiconductor. *Phys. Rev. Lett.* **2010**, ***105*****,** 136805−1−4.
14. Lee, C.; Yan, H.; Brus, L. E.; Heinz, T. F.; Hone, J.; Ryu, S. Anomalous Lattice Vibrations of Single- and Few-Layer MoS_2. *ACS Nano* **2010**, *4***,** 2695−2700.
15. Korn, T.; Heydrich, S.; Hirmer, M.; Schmutzler, J.; Schüller, C. Low-Temperature Photocarrier Dynamics in Monolayer MoS_2. *Appl. Phys. Lett.* **2011**, *99*, 102109−1−3.
16. Ghatak, S.; Pal, A. N.; Ghosh, A. Nature of Electronic States in Atomically Thin MoS_2 Field-Effect Transistors. *ACS Nano* **2011**, *5***,** 7707−7712.
17. Eda, G.; Yamaguchi, H.; Voiry, D.; Fujita, T.; Chen, M.; Chhowalla, M. Photoluminescence from Chemically Exfoliated MoS_2. *Nano Lett.* **2011**, *11***,** 5111−5116.
18. Zeng, H.; Dai, J.; Yao, W.; Xiao, D.; Cui, X. Valley Polarization in MoS_2 Monolayers by Optical Pumping. *Nat. Nanotechnol.* **2012**, *7***,** 490−493.
19. Mak, K. F.; He, K.; Shan, J.; Heinz, T. F. Control of Valley Polarization in Monolayer MoS_2 by Optical Helicity. *Nat. Nanotechnol.* **2012**, *7*, 494−498.
20. Mak, K. F.; He, K.; Lee, C.; Lee, G. H.; Hone, J.; Heinz, T. F.; Shan, J. Tightly Bound Trions in Monolayer MoS_2. *Nat. Mater.* **2013**, *12*, 207−211.
21. Kashid, R. V.; Late, D. J.; Chou, S. S.; Huang, Y.-K.; De, M.; Joag, D. S.; More, M. A.; Dravid, V. P. Enhanced Field-Emission Behavior of Layered MoS_2 Sheets. *Small* **2013**, *9*, 2730–2734.
22. Kim, S.; Konar, A.; Hwang, W.-S.; Lee, J. H.; Lee, J.; Yang, J.; Jung, C.; Kim, H.;

Yoo, J.-B.; Choi, J.-Y.; *et al.* High-Mobility and Low-Power Thin-Film Transistors Based on Multilayer MoS_2 Crystals. *Nat. Commun.* **2012**, *3*, 1011−1−7.

23. Yu, W. J.; Li, Z.; Zhou, H.; Chen, Y.; Wang, Y.; Huang, Y.; Duan, X. Vertically Stacked Multi-Heterostructures of Layered Materials for Logic Transistors and Complementary Inverters. *Nat. Mater.* **2013**, 12, 246−252.
24. Lin, J. D.; Zhong, J. Q.; Zhong, S.; Li, H.; Zhang, H. Modulating Electronic Transport Properties of MoS_2 Field Effect Transistor by Surface Overlayers. *Appl. Phys. Lett.* **2013**, *103*, 063109−1−4.
25. Lopez-Sanchez, O.; Lembke, D.; Kayci, M.; Radenovic, A.; Kis, A. Ultrasensitive Photodetectors Based on Monolayer MoS_2. *Nat. Nanotechnol.* **2013**, *8*, 497−501.
26. Bernardi, M.; Palummo, M.; Grossman, J. C. Extraordinary Sunlight Absorption and One Nanometer Thick Photovoltaics Using Two-Dimensional Monolayer Materials. *Nano Lett.* **2013**, *13*, 3664−3670.
27. Fontana, M.; Deppe, T.; Boyd, A. K.; Rinzan, M.; Liu, A. Y.; Paranjape, M.; Barbara, P. Electron-Hole Transport and Photovoltaic Effect in Gated MoS_2 Schottky Junctions. *Sci. Rep.* 2013, 3, 1634−1−5.
28. Britnell, L.; Ribeiro, R. M.; Eckmann, A.; Jalil, R.; Belle, B. D.; Mishchenko, A.; Kim, Y.-J.; Gorbachev, R. V.; Georgiou, T.; Morozov, S. V. *et al.* Strong Light-Matter Interactions in Heterostructures of Atomically Thin Films. *Science* **2013**, *340*, 1311−1314.
29. Ross, J. S.; Klement, P.; Jones, A. M.; Ghimire, N. J.; Yan, J.; Mandrus, D. G.; Taniguchi, T.; Watanabe, K.; Kitamura, K.; Yao, W. *et al.* Electrically Tunable Excitonic Light-Emitting Diodes Based on Monolayer WSe_2 P–N Junctions. *Nat. Nanotechnol.*2014, **9**, 268−272.
30. Chang, Y.-H.; Lin, C.-T.; Chen, T.-Y.; Hsu, C.-L.; Lee, Y.-H.; Zhang, W.; Wei, K.-H.; Li, L.-J. Highly Efficient Electrocatalytic Hydrogen Production by MoSx Grown on Graphene-Protected 3D Ni Foams. *Adv. Mater.* **2013**, *25*, 756−760.
31. Chang, Y.-H.; Wu, F.-Y.; Chen, T.-Y.; Hsu, C.-L.; Chen, C.-H.; Wiryo, F.; Wei, K.-H.; Chiang, C.-Y.; Li, L.-J. Three-Dimensional Molybdenum Sulfide Sponges for Electrocatalytic Water Splitting. Small 2014, 10, 895−900.
32. Xiang, Q.; Yu, J.; Jaroniec, M. Synergetic Effect of MoS_2 and Graphene as Cocatalysts for Enhanced Photocatalytic H_2 Production Activity of TiO_2 Nanoparticles. *J. Am. Chem. Soc.* **2012**, **134**, 6575−6578.
33. Zhang, W.; Huang, J.-K.; Chen, C.-H.; Chang, Y.-H.; Cheng, Y.-J.; Li, L.-J. High-Gain Phototransistors Based on a CVD MoS_2 Monolayer. *Adv. Mater.* **2013**, *25*, 3456–3461.
34. Zhang, W.; Chuu, C.-P.; Huang, J.-K.; Chen, C.-H.; Tsai, M.-L.; Chang, Y.-H.; Liang, C.-T.; Chen, Y.-Z.; Chueh, Y.-L.; He, J.-H. *et al.* Ultrahigh-Gain Photodetectors Based on Atomically Thin Graphene-MoS_2 Heterostructures. *Sci. Rep.* **2014,** *4*, 3826−1−8.
35. Tongay, S.; Zhou, J.; Ataca, C.; Lo, K.; Matthews, T. S.; Li, J.; Grossman, J. C.; Wu, J. Thermally Driven Crossover from Indirect toward Direct Bandgap in 2D Semiconductors: $MoSe_2$ versus MoS_2. *Nano Lett.* **2012**, *12*, 5576−5580.
36. Horzum, S.; Sahin, H.; Cahangirov, S.; Cudazzo, P.; Rubio, A.; Serin, T.; Peeters, F. M. Phonon Softening and Direct to Indirect Band Gap Crossover in Strained Single-Layer $MoSe_2$. *Phys. Rev. B* **2013**, *87*, 125415−1−5.

37. Ross, J. S.; Wu, S.; Yu, H.; Ghimire, N. J.; Jones, A. M.; Aivazian, G.; Yan, J.; Mandrus, D. G.; Xiao, D.; Yao, W. *et al.* Electrical Control of Neutral and Charged Excitons in a Monolayer Semiconductor. *Nat. Commun.* **2013**, *4*, 1474−1−6.
38. Tonndorf, P.; Schmidt, R.; Böttger, P.; Zhang, X.; Börner, J.; Liebig, A.; Albrecht, M.; Kloc, C.; Gordan, O.; Zahn, D. R. T. *et al.* Photoluminescence Emission and Raman Response of Monolayer MoS_2, $MoSe_2$, and WSe_2. *Opt. Express* **2013**, *21*, 4908−4916.
39. Kang, J.; Tongay, S.; Zhou, J.; Li, J.; Wu, J. Band Offsets and Heterostructures of Two-Dimensional Semiconductors. *Appl. Phys. Lett.* **2013**, *102*, 012111−1−4.
40. Lee, C.; Yan, H.; Brus, L. E.; Heinz, T. F.; Hone, J.; Ryu, S. Anomalous Lattice Vibrations of Singleand Few-Layer MoS_2. *ACS Nano* **2011**, *5*, 2695–2700.
41. Zeng, H.; Liu, G.-B.; Dai, J.; Yan, Y.; Zhu, B.; He, R.; Xie, L.; Xu, S.; Chen, X.; Yao, W. *et al.* Optical Signature of Symmetry Variations and Spin-Valley Coupling in Atomically Thin Tungsten Dichalcogenides. *Sci. Rep.* **2013,** *3*, 1608−1−5.
42. Abdallah, W. A.; Nelson, A. E. Characterization of $MoSe_2$(0001) and Ion-Sputtered $MoSe_2$ by XPS. *J. Mater. Sci.* **2005**, *40***,** 2679–2681.
43. Pouzet, J.; Bernede, J. C. $MoSe_2$ Thin Films Synthesized by Solid State Reactions between Mo and Se Thin Film. *Revue Phys. Appl.* **1990**, *25*, 807−815.
44. Larentis, S.; Fallahazad, B.; Tutuc, E. Field-Effect Transistors and Intrinsic Mobility in Ultra-Thin $MoSe_2$ Layers. *Appl. Phys. Lett.* **2012**, *101*, 223104−1−4.
45. Wu, C.I.; Kahn, A. Investigation of the Chemistry and Electronic Properties of Metal/Gallium Nitride Interfaces. *J. Vaccum Sci & Tech B* **1998**, 16, 2218−2223.
46. Chen M.H.; Wu C.I. Roles of Thermally Evaporated Cesium Oxide in Organic Light Emitting Diodes. *J. Appl. Phys*. **2008**, *104*, 113713−1−4.
47. Chen, C.-Y.; Retamal, J. R. D.; Wu, I.-W.; Lien, D.-H.; Chen, M. W.; Ding, Y.; Chueh, Y.-L.; Wu, C.-I.; He, J.-H. Probing Surface Band Bending of Surface-Engineered Metal Oxide Nanowires. *ACS Nano* **2012**, *6*, 9366−9372.
48. Schlaf, R.; Lang, O.; Pettenkofer, C.; Jaegermann, W. Band Lineup of Layered Semiconductor Heterointerfaces Prepared by Van Der Waals Epitaxy: Charge Transfer Correction Term for The Electron Affinity Rule. *J. Appl. Phys.* **1999**, *85*, 2732−2753.
49. Choi, M. S.; Lee, G.-H.; Yu, Y.-J.; Lee, D.-Y.; Lee, S. H.; Kim, P.; Hone, J.; Yoo, W. J. Controlled Charge Trapping by Molybdenum Disulphide and Graphene in Ultrathin Heterostructured Memory Devices. *Nat. Commun.* **2013**, *4*, 1624−1−7.
50. Fu, D.; Zhou, J.; Tongay, S.; Liu, K.; Fan, W.; Liu, T.-J. K.; Wu, J. Mechanically Modulated Tunneling Resistance in Monolayer MoS_2. *Appl. Phys. Lett.* **2013**, *103*, 183105−1−3.
51. Kang, J.; Tongay, S.; Zhou, J.; Li, J.; Wu, J. Band Offsets and Heterostructures of Two-Dimensional Semiconductors. *Appl. Phys. Lett.* **2013**, *102*, 012111−1−4.
52. Yin, Z.; Li, H.; Li, H.; Jiang, L.; Shi, Y.; Sun, Y.; Lu, G.; Zhang, Q.; Chen, X.; Zhang, H. Single-Layer MoS_2 Phototransistors. *ACS Nano*, **2012**, *6*, 74–80.
53. Tongay, S.; Suh, J.; Ataca, C.; Fan, W.; Luce, A.; Kang, J. S.; Liu, J.; Ko, C.; Raghunathanan, R.; Zhou, J. *et al.* Defects Activated Photoluminescence in Two-Dimensional Semiconductors: Interplay between Bound, Charged, and Free Excitons. *Sci. Rep.* **2013,** *3*, 2657−1−5.
54. Zhang, A.; You, S.; Soci, C.; Liu, Y.; Wang, D.; Lo, Y.-H. Silicon Nanowire Detectors Showing Phototransistive Gain. *Appl. Phys. Lett.* **2008**, *93*, 121110−1−3.

55. Lany, S.; Zunger, A. Anion Vacancies as a Source of Persistent Photoconductivity in II-VI and Chalcopyrite Semiconductors. *Phys. Rev. B* **2005**, *72*, 035215−1−13.

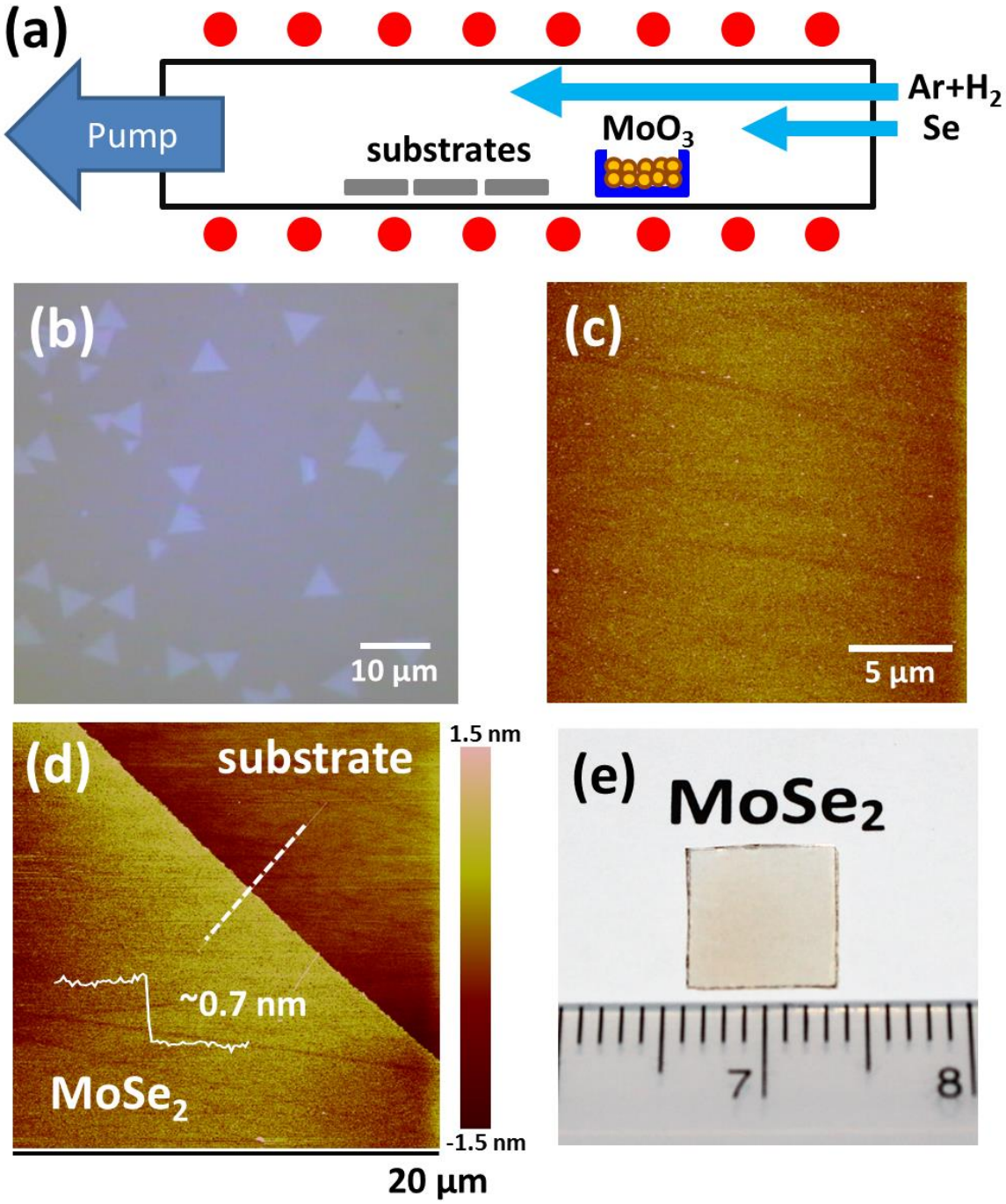

Figure 1. (a) Schematic illustration for the growth of $MoSe_2$ layers on sapphire substrates by the selenization of MoO_3 powders in a CVD furnace. (b,c) The AFM images of the monolayer $MoSe_2$ flakes and monolayer film grown at 800 ˚C, where the difference is the

location of the substrates in furnace. (d) AFM image, and (e) OM of a monolayer $MoSe_2$ film grown at 800 °C on a sapphire substrate.

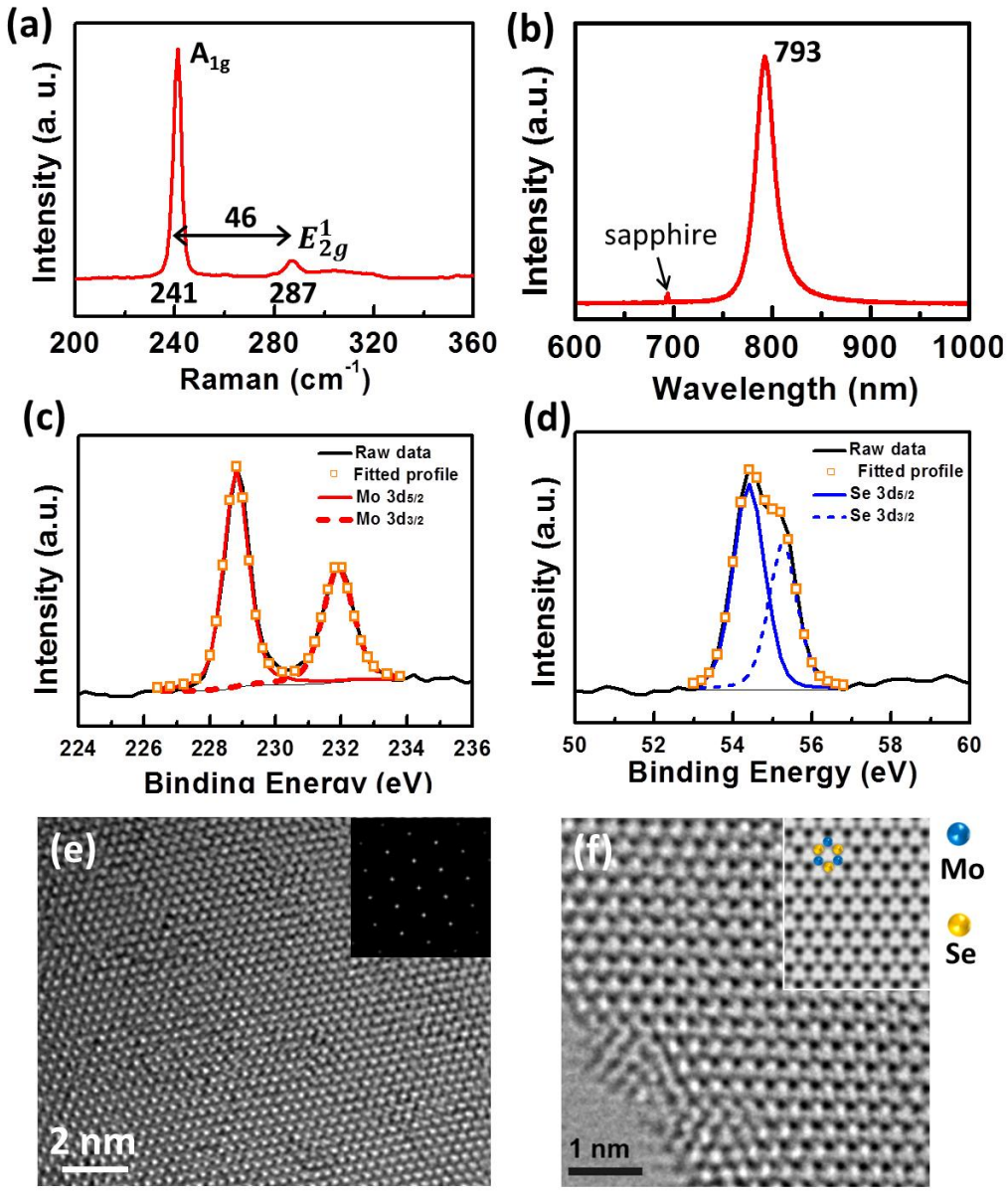

Figure 2. (a) Raman spectrum for the monolayer $MoSe_2$, obtained in a confocal Raman spectrometer excited by a 473 nm laser. (b) Photoluminescence spectra for the CVD monolayer $MoSe_2$, obtained in a microscopic PL system (excitation wavelength 532 nm). (c,d) XPS spectra of the monolayer $MoSe_2$ film, where the (c) Mo 3d and (d) Se 3d binding energies are identified. (e) High resolution TEM image of monolayer $MoSe_2$ with

an inset showing its Fourier transform pattern. (f) Enlarged TEM image, where the Mo and Se atoms are identified. The inset is a simulated HRTEM image of monolayer $MoSe_2$.

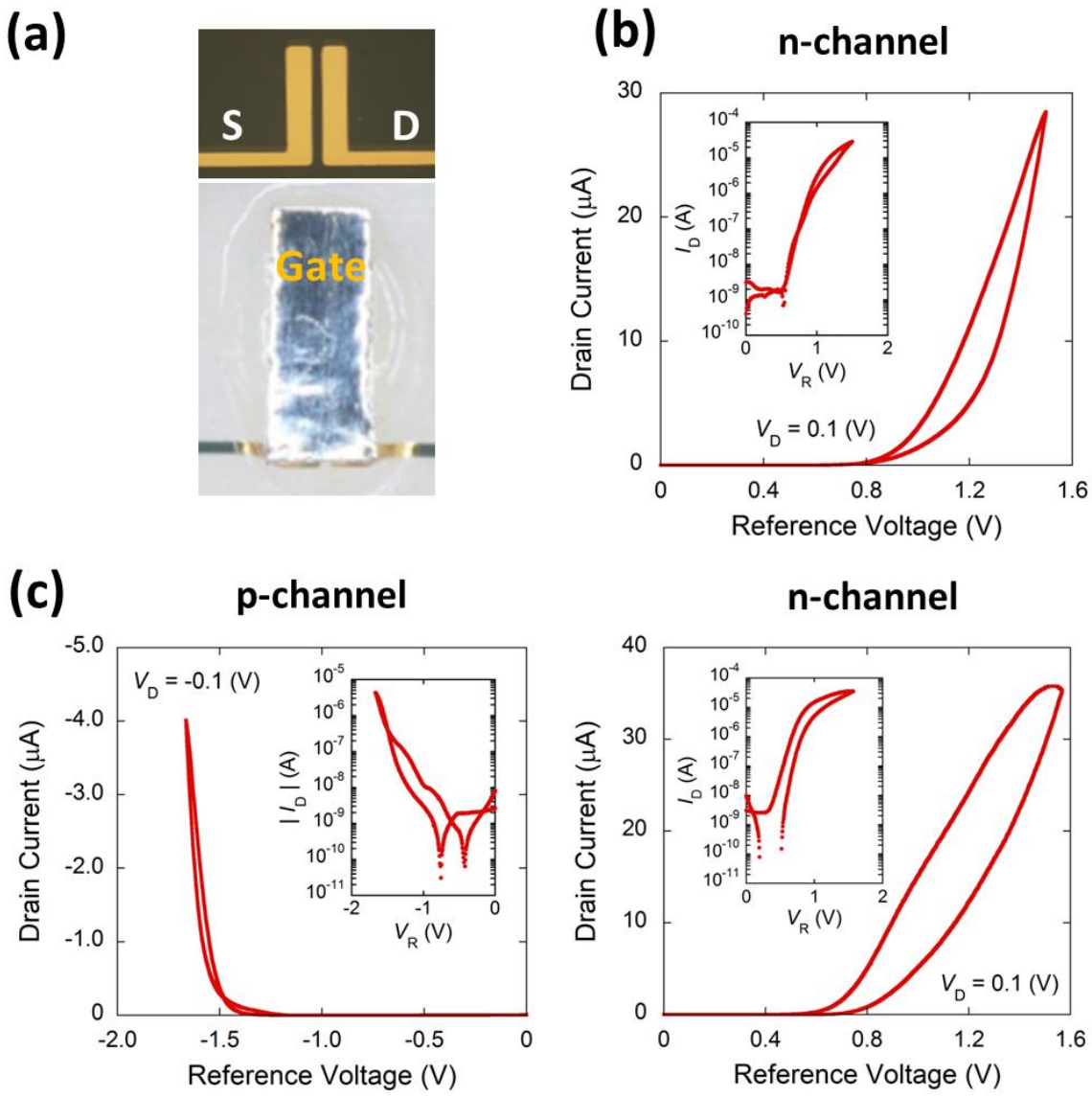

Figure 3. (a) Optical micrograph (top view) for the $MoSe_2$ EDLT device, where the top and bottom photos were taken before and after the ion gel/top gate deposition. (b,c) The typical transfer curves of the (b) MoS_2 and (c) $MoSe_2$ EDLT devices, where the inset in each graph shows the transfer curve plotted in a log scale.

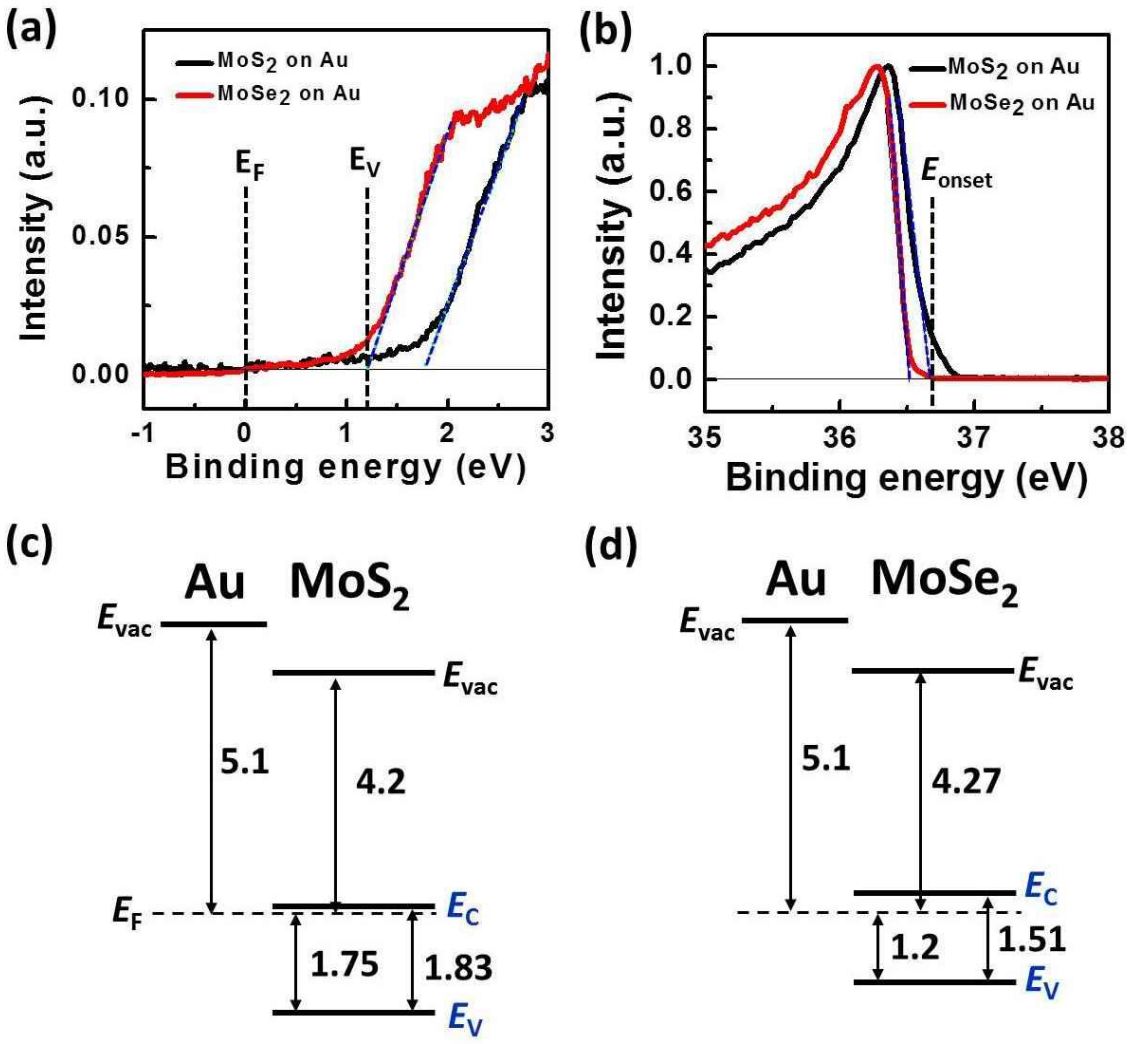

Figure 4. Ultraviolet photoemission spectroscopy and energy band diagrams. (a) UPS spectra, near the Fermi level energy and valence band maximum, of the monolayer MoS_2 and $MoSe_2$ film transferred onto the 60 nm Au-coated Si substrates. (b) The onset level (E_{onset}) of the UPS spectra, where the work function (Φ) can be calculated by $\Phi = h\nu - E_{onset}$. $h\nu$ is the incident photon energy of 40.8 eV. (c,d) Energy band diagrams of the monolayer (c) MoS_2 and (d) $MoSe_2$ film, where Au metal is used as a reference. Note that the band gap energies used in diagram are optical gaps.

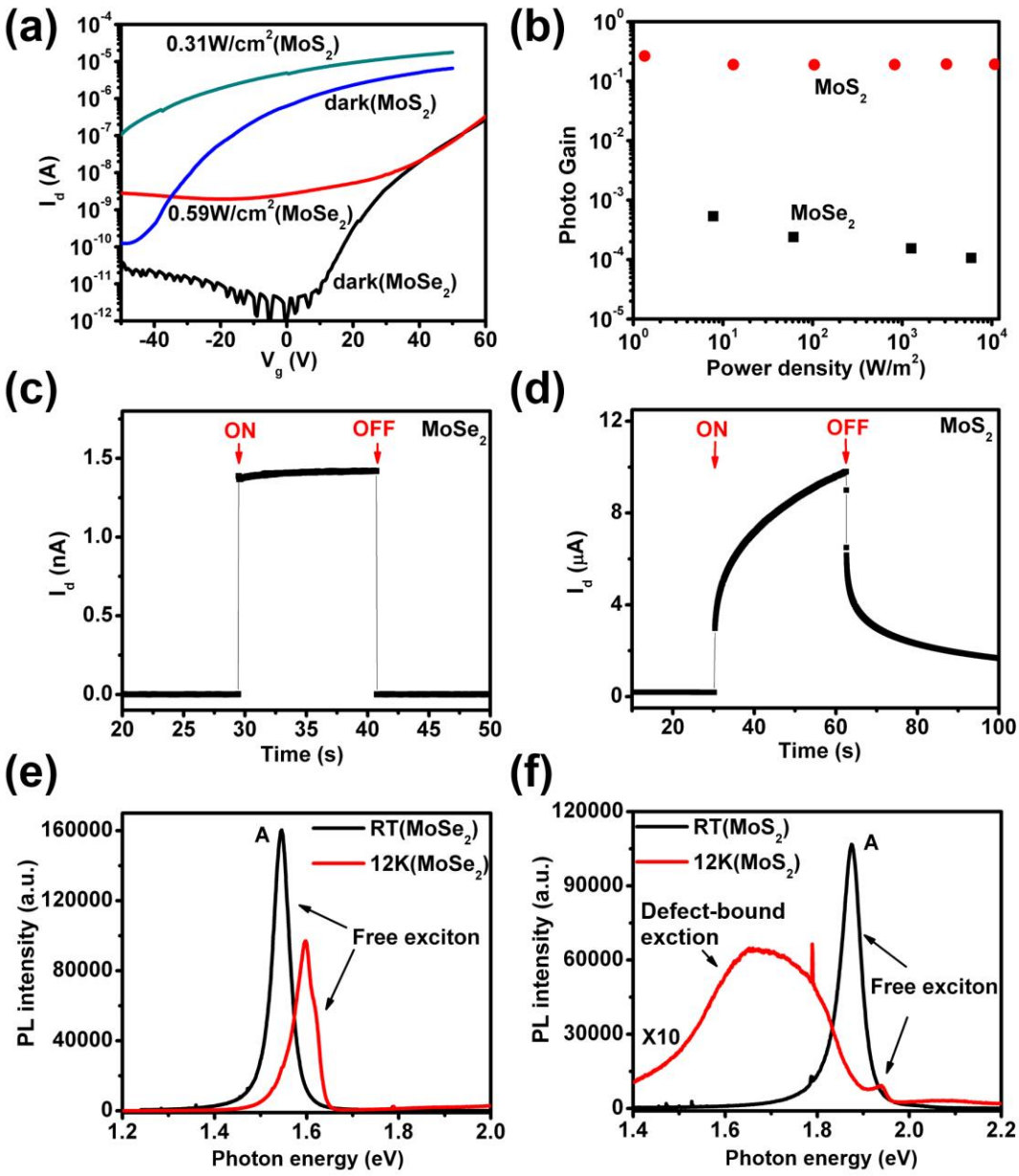

Figure 5. Optical properites of CVD $MoSe_2$ and MoS_2 monolayers. (a) I_d-V_g transfer characteristics of the photodetectors based on CVD $MoSe_2$ and MoS_2 monolayers in dark and under illumination at V_{ds} = 1 V. (b) The power density dependence of the photo gain at V_{ds} = 1 V for the photodetectors at the OFF state, where V_g is 0 V for the $MoSe_2$ and V_g is -48 V for the MoS_2. (c,d) Time-resolved photocurrents of the photodectors based on $MoSe_2$ at P = 0.59 W/cm^2 and MoS_2 at P = 0.31 W/cm^2, respectively. (e,f) The PL spectra of monolayer $MoSe_2$ and MoS_2, respectively, at room temperature (RT) and 12 K.

Table 1. The summarization of the MoS_2 and $MoSe_2$ from EDLT measurments.

	Mobility (cm^2/Vs)		On/Off	type
	Hole	Electron		
MoS_2	**–**	**~17**	**10^4-10^5**	**n-type**
$MoSe_2$	**~15**	**~23**	**10^4-10^5**	**Ambipolar***

***n-type preferred**